Journal of Solid State Chemistry 323 (2023) 123926

Contents lists available at ScienceDirect

Journal of Solid State Chemistry

journal homepage: www.elsevier.com/locate/jssc

Structure redetermination, transport and thermal properties of the YNi_3Al_9 compound

Igor Oshchapovsky [a,b,*], Ebube E. Oyeka [c], Thao T. Tran [c], Tomasz Klimczuk [a], Michał J. Winiarski [a]

[a] Faculty of Applied Physics and Mathematics and Advanced Materials Center, Gdansk University of Technology, Gabriela Narutowicza Str. 11/12, 80-233, Gdansk, Poland
[b] Department of Inorganic Chemistry, Ivan Franko National University of Lviv, Kyryla i Mefodiya Str. 6, 79005, Lviv, Ukraine
[c] Department of Chemistry, Clemson University, Clemson, SC, 29630, United States

ARTICLE INFO

Keywords:
Intermetallics
Rare earth alloys and compounds
Crystal growth
Crystal structure
Electrical transport
Heat capacity
Magnetoresistance
X-ray diffraction

ABSTRACT

Single crystals of completely ordered variant of the YNi_3Al_9 compound were grown by self-flux method with excess of aluminum. The crystal structure of the title compound was redetermined from single crystal X-ray diffraction data. The structure adopts $ErNi_3Al_9$ type, space group *R32*, parameters of the unit cell a = 7.2838(2) Å, c = 27.4004(8) Å. The growth of relatively large single crystals of the YNi_3Al_9 compound, having completely ordered structure, indicates possible existence of region on phase diagram, where the title compound is in equilibrium with liquid. Comparison with the results in the literature on the investigations of the same and related compounds shows trend towards formation of more ordered structures in flux grown samples and more disordered ones in arc melted samples.

Physical properties of the title compound - electrical resistivity, magnetoresistance and heat capacity - were measured for the first time. It shows metallic-like behavior with very high values of magnetoresistance up to 420% at low temperatures without presence of magnetic elements. Therefore electronic structure calculations were carried out. The phonon heat capacity reveals major Debye and minor Einstein contributions at the intermediate temperatures, and total heat capacity approaches Dulong-Petit limit at high temperatures. The calculated Debye temperature from the whole temperature range θ_D = 480(6) K is typical for aluminium-rich compounds. Corresponding Einstein temperature is θ_E = 198(8) K. The estimations of electron-phonon coupling constant λ = 0.092 show very weak coupling and absence of superconducting transition.

1. Introduction

The aluminum alloys possess wide range of properties, causing their wide application from structural materials [1] to magnetic cores [2]. The aluminum alloys attract attention both because of their practical application and from fundamental point of view. Among them are amorphous alloys R-{Fe,Ni}-Al [3], quasicrystals [4], Kondo systems [5] (many RT_2Al_{20} compounds adopting $CeCr_2Al_{20}$ structure type [6]). The latter structure type facilitates to the existence of soft modes of atomic oscillations.

The compounds RNi_3Al_9 (R = rare-earth metal Y, Gd, Tb, Dy, Er, Yb, Lu) attract attention because of their chiral polar space group structures, uncommon in general [7,8], potentially resulting in non-trivial spin textures or possible triplet superconductivity [9]. Chiral intermetallics also attract attention as possible catalysts for the stereoselective synthesis [10].

The structure of the RNi_3Al_9 compounds consists of alternating layers with compositions R_2Al_3, Ni, and Al. The closest R-R distances inside R_2Al_3 layers are ~4.2 Å and are much shorter than corresponding distances between these layers ~9.13 Å. It is these almost two times shorter intralayer R-R distances that cause 2D-like magnetic behavior in these, as the rare-earth metals are the only atoms with magnetic moment there. The comparison of compounds having non-magnetic atom (Y in the title compound, Lu) with ones hosting a magnetic rare-earth metals can help to study the electronic, lattice, and magnetic properties.

Several RNi_3Al_9 compounds were studied by Gladyshevskyy et al.

* Corresponding author. Faculty of Applied Physics and Mathematics and Advanced Materials Center, Gdansk University of Technology, Gabriela Narutowicza Str. 11/12, 80-233, Gdansk, Poland.
E-mail address: ihor.oshchapovskyy@lnu.edu.ua (I. Oshchapovsky).

https://doi.org/10.1016/j.jssc.2023.123926
Received 28 November 2022; Received in revised form 10 February 2023; Accepted 15 February 2023
Available online 3 March 2023

[11] (R = Er, Gd, Dy, Y) Matselko et al. (R = Sc, Y, Gd-Lu) [12], Yamashita et al. [13], moreover, the investigations of physical properties were done for R = Tb, Er by S.G. de Mercena [14,15] and R = Yb, which attracted much attention due to its difference from other rare earths (see Yamashita et al. [13] and Tobash et al. [16].). Yb-containing compounds, in addition to competing Rudeman-Kittel-Kasui-Yosida and Kondo interactions can have variable valence, leading to interesting phenomena, e.g. valence state fluctuations.

The physical properties of YNi_3Al_9 had not been investigated before, this was done in our publication for the first time. Unfortunately, most of the diffraction studies of the 1:3:9 compounds except Gladyshevskyy et al. [11] and Tobash et al. [16] were done using powder data only. This implies that small details of the structure cannot be established completely well. Thus the question remains which structural model of YNi_3Al_9 is correct: an ordered one with space group *R32* as in Gladyshevskyy et al. [11], a disordered *P-6m2* as in Matselko et al. [12], or a variant with stacking faults. Another important aspect is possible influence of the disorder of the atoms of the rare earths on physical properties. Therefore it is very desirable to determine crystal structures accurately before comparing measured physical properties.

One should also admit some discrepancies between isothermal sections of the phase diagram of the Y–Ni–Al, obtained by different authors: Mika et al. [17], Raggio et al. [18] and Huang et al. [19]. The most important difference is whether there is equilibrium between liquid phase and the title compound.

The article consists of two parts – crystal structure redetermination and measurements of physical properties.

2. Experimental

2.1. Synthesis

The sample with mass ~1 g was made starting from pure elements - yttrium (Onyxmet, dendritic, purity 99.99 wt%, stored in a glovebox under protective Ar atmosphere), nickel (Alfa Aesar, purity >99.95 wt%) and aluminum (OnyxMet, purity 99.99 wt%) by self-flux method with composition Y:Ni:Al = 1:3:20 using excess aluminum as flux. Small pieces of metals were put into alumina crucible, covered by perforated alumina cap and additional empty crucible and finally sealed into quartz ampoule with argon atmosphere under pressure 20 mbar. The ampoule was put into the furnace, heated to 200 °C, then heated to 1050 °C with a temperature rate 150 °C/h, held for 24 h, and slowly cooled to 750 °C at 3 °C/h. Then the excess Al flux was removed from alloy into the additional crucible by centrifugation for several minutes until solidification of aluminium and let cool without breaking the ampoule.

2.2. Structure investigations

Small good quality single crystals were obtained from sample YNi_3Al_{20} by mechanical fragmentation. They were selected from parts, having rhombohedral shape. That alloy also contained small amount of $Y_3Ni_5Al_{19}$, having needle-like shape. Single crystal diffraction data were collected using Bruker APEX-II CCD (Mo K_α radiation, graphite monochromator) single crystal diffractometer. Data collection, determining of the unit cell, integration, data reduction and absorption correction were done using Bruker SAINT software [20]. The collection of powder data from all the samples was carried out using Bruker D2 Phaser powder diffractometer (Cu K_α radiation) for subsequent phase analysis using program Eva and PDF4+ database. The preliminary analysis of systematic extinctions was done by program XPrep [21]. The solution of crystal structure and determination of symmetry of electronic density map was done by program Superflip [22], the refinement of the structure from single crystal diffraction data was done using program Jana2006 [23], using Becker-Coppens type 1 Gaussian isotropic extinction [24,25].

2.3. Measurements of physical properties

Physical properties measurements were performed on the PPMS Evercool II system (Quantum Design). Temperature and magnetic field dependence of electrical resistivity was measured using a dc four-point technique in the temperature range T = 2–300 K. Long platelet-like specimen was prepared by polishing rhombohedral single crystal, highly elongated along the *c* direction (here the hexagonal notation of the unit cell is used). The electrical leads, made from 25 μm platinum wires, were spot-welded to the sample. The direction of current was approximately perpendicular to *a* axis. Electrical leads, made from 25 μm platinum wires, were attached to the sample by capacitor spot welding. Heat capacity studies were undertaken in zero field using a standard thermal relaxation technique in the temperature range 1.9 K < T < 300 K.

2.4. Electronic structure calculations

The electronic structure of the title compound was calculated using program JDFTx [26], GBRV [27] pseudopotential library and Perdew-Zunger LDA exchange-correlation functional [28] with the cutoff energies of plane waves equal to 40 Hartree on unrelaxed structure of the YNi_3Al_9 compound (rhombohedral setting) on 8 × 8 × 8 k-point mesh without explicit treatment of spins. The convergence energy threshold was equal 1E-8 Hartree. Linear-tetrahedron sampling method for density of states was employed [29].

3. Results and discussion

3.1. Crystal structure and phase formation

Almost pure sample was obtained by self-flux technique using excess aluminum as a flux. The sample contained single crystals of the title compound as the main phase and small amount of $Y_3Ni_5Al_{19}$ needles after the removal of liquid aluminum flux by centrifugation. The single crystals had rhombohedral shape and were several millimeters long with aspect ratio approx. 3:1. The growth of large good quality single crystals clearly indicates that there is region on the phase diagram, where YNi_3Al_9 is in equilibrium with liquid phase at least in some temperature range. This is in contrast with publications by Raggio et al. [18], Huang et al. [19] and indirectly supports publication by Mika et al. [17] and indicates that the system Y–Ni–Al is not yet completely investigated. In principle it is even possible that in some systems metastable equilibria exist where the resulting phases at definite temperature depend on previous thermal history of samples.

It should be noted that some samples of the RNi_3Al_9 compounds, presented in the literature, differ in one detail – the presence or absence of numerous highly broadened diffraction peaks. This phenomenon was observed and described by Matselko et al. [12]. The problem was that most of the broadened peaks were difficult or impossible to describe neither by conventional rhombohedral unit cell $a_r \approx 7.3$ Å, $c_r \sim 27.4$ Å[1] nor by smaller hexagonal unit cell, discussed below. Gladyshevskyy et al. [11] in his work, devoted to RNi_3Al_9 compounds, previously proposed that those compounds could be derived from some hypothetic disordered structure, having space group *P-6m2* and smaller unit cell $a_h \approx 4.2$ Å, $c_h \sim 9.1$ Å with the following relations between both unit cells $a_r = \sqrt{3}a_h$ and $c_r = 3c_h$. Matselko et al. [12] in their work, devoted mainly to $YbNi_3Al_9$, concluded from the refinement using powder diffraction data, that arc-melted $YbNi_3Al_9$ adopts disordered hexagonal structure (denoted as $Yb_{0.67}Ni_2Al_6$) with a small unit cell and space group *P-6m2*. As for other compounds RNi_3Al_9 (R = Sc, Y, Gd–Tm, Lu), studied by Matselko et al. [12], only the refinement of the parameters of the disordered smaller variant of the unit cell in space group *P-6m2* was done. They assumed

[1] Here parameters of the rhombohedral unit cell have indices "r", while parameters of the hexagonal unit cell have indices "h".

that the compounds may adopt different variants of the structure, depending on the synthesis route.

The question, which model of the structure is more appropriate stimulated the reinvestigation of the structure of the YNi_3Al_9 compound. Therefore small fragments of the single crystals of the title compound, grown by self-flux were selected for further collection of the single crystal X-ray diffraction data. The obtained results clearly indicated, that in our particular case, the YNi_3Al_9 single crystal, grown from Al flux (Y:Ni:Al = 1:3:20), had a larger unit cell with a = 7.2838(2) Å, c = 27.4004(8) Å, $\alpha = \beta = 90°$ and $\gamma = 120°$. While the unit cell had hexagonal metric, the correct determination of the symmetry of the unit cell was an another issue. The main reason of this was specific motif of the structure of RNi_3Al_9 compounds. They consist of three types of monoatomic layers: R_2Al_3 with alternating R atoms and Al_3 triangles, triangular mesh Ni_3 and triangular mesh Al_3 (Gladyshevskyy et al. [11]). The completely ordered rhombohedral structure of $ErNi_3Al_9$ type (space group *R32*) has 24 layers, stacked in the following sequence: $(Al_3–Al_3–Ni_3–Al_3-R_2Al_3–Al_3–Ni_3–Al_3)_3$ or after reordering $(R_2Al_3–Al_3–Ni_3–Al_3–Al_3–Al_3–Ni_3–Al_3)_3$. The completely disordered hexagonal structure (space group *P-6m2*), like that, predicted in Gladyshevskyy et al. [11] or determined by Matselko et al. [12] for $YbNi_3Al_9$ has similar stacking sequence of layers $R_2Al_3–Al_3–Ni_3–Al_3–Al_3–Al_3–Ni_3–Al_3$. The structures of $DyNi_3Al_9$ and YNi_3Al_9 compounds, published by Gladyshevskyy et al. [11] were partially disordered, but still retained larger rhombohedral unit cells. All the aforementioned structures have similar motifs – namely similar shape of the Al and Ni monoatomic layers and similar fragment $R_2Al_3–Al_3–Ni_3–Al_3–Al_3–Al_3–Ni_3–Al_3$ in stacking sequence. The most significant difference is the degree of ordering of the R_2Al_3 layers. All R_2Al_3 layers consist of alternating R atoms of the rare earths and Al_3 triangles. The ordering decreases in row $ErNi_3Al_9$>$DyNi_3Al_9$>$YbNi_3Al_9$. It was shown in Gladyshevskyy et al. [11], that maximum amount of the Al_3 triangles in the R_2Al_3 layer corresponds to the full ordering and composition R_2Al_3 as otherwise the shortest Al–Al distances make such configurations impossible. There are two possibilities of the disorder – larger rare earth content and/or different stacking of the completely ordered R_2Al_3 layers. The positions of the layers in *xy* plane are fixed to coordinates (0 0), (1/3 2/3) and (2/3 1/3), taking position of R as the basis. Stacking layers in such way that R and Al_3 are distributed completely in random order among possible xy positions (0 0), (1/3 2/3) and (2/3 1/3) leads to smaller unit cell with space group *P-6m2*. Stacking layers one upon another leads to bigger unit cell with space group *P-6m2* (structure relations are shown in Fig. 1). Another aspect is pseudosymmetry, namely the positions of atoms in the $ErNi_3Al_9$-type structures are very close to the "ideal" positions for the space group *P-6m2*. All this, together with very small shifts of atoms, determines the unit cell and symmetry.

Two approaches were employed in determination of the symmetry – from systematic extinctions and from symmetry of the electronic density map. The presence of pseudosymmetry made determination of the space group difficult, because for each Laue group R_{int} was almost the same (Tables S1–S3). Taking into the account hexagonal metric of the unit cell, it was better to focus on trigonal and hexagonal Laue groups. The preliminary analysis of systematic extinctions by program Jana2006 [23] showed that R centering was the most favorable in case of trigonal groups *-3* and *-3m1*, the all groups where it was possible. The mean $|E^*E^{-1}|$ value, calculated by program XPREP, was 1.097, meaning that the compound was most likely centrosymmetric, as it was closer to expected value 0.968 for a centrosymmetric spacegroup, than to 0.736 for a non-centrosymmetric one. XPREP also confirmed possibility of R centering, the existence of 3_2 screw axis and suggested centrosymmetric space group *R-3* as the most appropriate. Later solution and refinement using this space group failed. Statistics analysis gave little additional information towards proper space group choise. Further analysis of systematic extinctions did not reveal any preferences among possible space groups. The solution of the structure and analysis of the symmetry of the electronic density map by program Superflip was not unambiguous too. Several space groups were suggested by Superflip (initial space group *P1*), depending on starting random phases: $P3_121$, *P-62m*, $P3_221$, $P3_2$, $P3_1$. Therefore space group with either *3* or 3_1, 3_2, axes of symmetry was expected (rhombohedral centering was not proposed automatically). Taking into the account lack of certainty in spacegroup determination, several attempts were made to solve the structure in space groups *P-6m2*, *P-62m, R3*, *R-3*, *R-3m*, *R32*, $P3_1$. The model in space group *R3* appeared the most favorable, while various centrosymmetric space groups rather failed. Subsequent check of the model in space group *R3* by program Platon [30] suggested higher symmetry space group *R32*. The initial model in space group *R3* was transformed to space group *R32* and further refined. Surprisingly, both models of the structure in space groups *R3* and *R32* described experimental data almost equally well without any large correlations in spite of *R3* being a subgroup of *R32* and additional *2, 2_1* axes in spacegroup *R32*. The results of the structure solution and refinement from single crystal diffraction data of both models in space groups *R32* and *R3* are presented in Tables S4–S8 in Supplementary Information. One should admit small difference between our results of structure determination of the title compound and those, published in Gladyshevskyy et al. [11]. The structure of YNi_3Al_9, synthesized by flux growth with excess of aluminum, is completely ordered in our case, while the structure of the crystal from arc-melted sample (Gladyshevskyy et al. [11]) has small disorder. This disorder is caused either by small excess of yttrium (however composition from the results of the refinement deviates negligibly from the ideal YNi_3Al_9) or, more likely in this case, by method of synthesis. Therefore strong sensitivity of structure towards composition and conditions of synthesis was apparent. Such subtle difference between two descriptions of one single crystal and strong sensitivity to the conditions of synthesis raised the question about possibility of modulation or any other structure peculiarities, as even the slightest change of composition, temperature, etc. can shift atoms and lead to symmetry change. The structure sensitivity towards synthesis conditions required careful attention to the details of the structure determination, mainly correct space group assignment and possibility of disorder. The analysis of diffraction patterns and reciprocal cell did not show any apparent satellites, diffuse scattering or other significant structural features, only some signs of twinning were visible (See Figs. S1–S5). The absolute configuration was tested for both models by the refinement of fraction of the inversion twin. The corresponding twin volume fractions, corresponding to Flack parameters were equal and close to zero for both models, indicating correct absolute configuration. The projections of the unit cells are presented in Fig. 2.

While models in both space groups describe single crystal experimental data almost equally well, model in space group *R32* is preferred due to higher symmetry, less refined parameters and slightly lower agreement factors (See Table S4).

The assumption by Matselko et al. [12] that different synthesis routes can lead to different structures can be substantiated in the following way. In addition to phase $Yb_{0.67}Ni_2Al_6$ (composition $YbNi_3Al_9$) synthesized by Matselko et al. [12], partially ordered variant of the $YbNi_3Al_{9.23}$ compound with close composition was found in flux-grown samples, studied by Tobash et al. [16]. The latter has defect structure of $ErNi_3Al_9$ type with additional Wyck. 3a (0 0 1/2) position of aluminum. In addition to those, our results of investigation of the *completely ordered flux-grown* YNi_3Al_9 compound in comparison with *slightly disordered arc-melted* YNi_3Al_9 compound clearly show, that there is trend towards formation of ordered phases in the course of flux growth, whereas arc melting can lead to more disordered ones. The possible explanation is that flux growth provides less temperature and concentration gradients, better diffusion through liquid flux in course of phase transformation, as well as excess aluminum facilitates better ordering inside R_2Al_3 layers as was discussed earlier. Therefore it is considered that both completely ordered variant ($ErNi_3Al_9$ type), slightly ordered ($DyNi_3Al_9$ type), completely disordered ($Yb_{0.67}Ni_2Al_6$ type) or that with stacking faults are possible, depending on synthesis route. In principle, the formation of stacking faults in layered structures may be caused both by synthesis conditions and by intensive grinding. This possibility was discussed more in detail in Refs. [31,32].

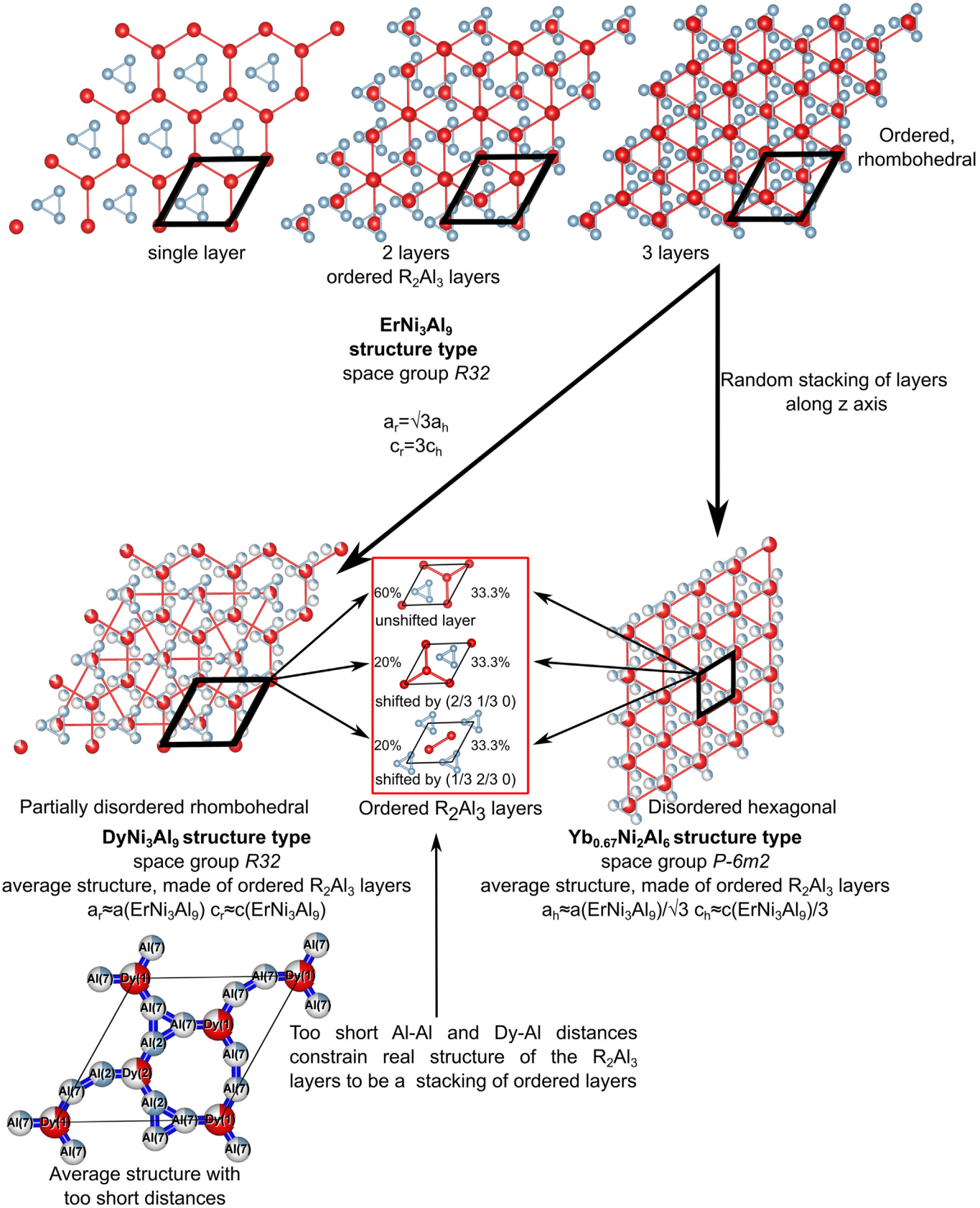

Fig.1. Structure relationship between R_2Al_3 layers in completely ordered $ErNi_3Al_9$ structure type, partially disordered $DyNi_3Al_9$ type and completely disordered $Yb_{0.67}Ni_2Al_6$ structure type.

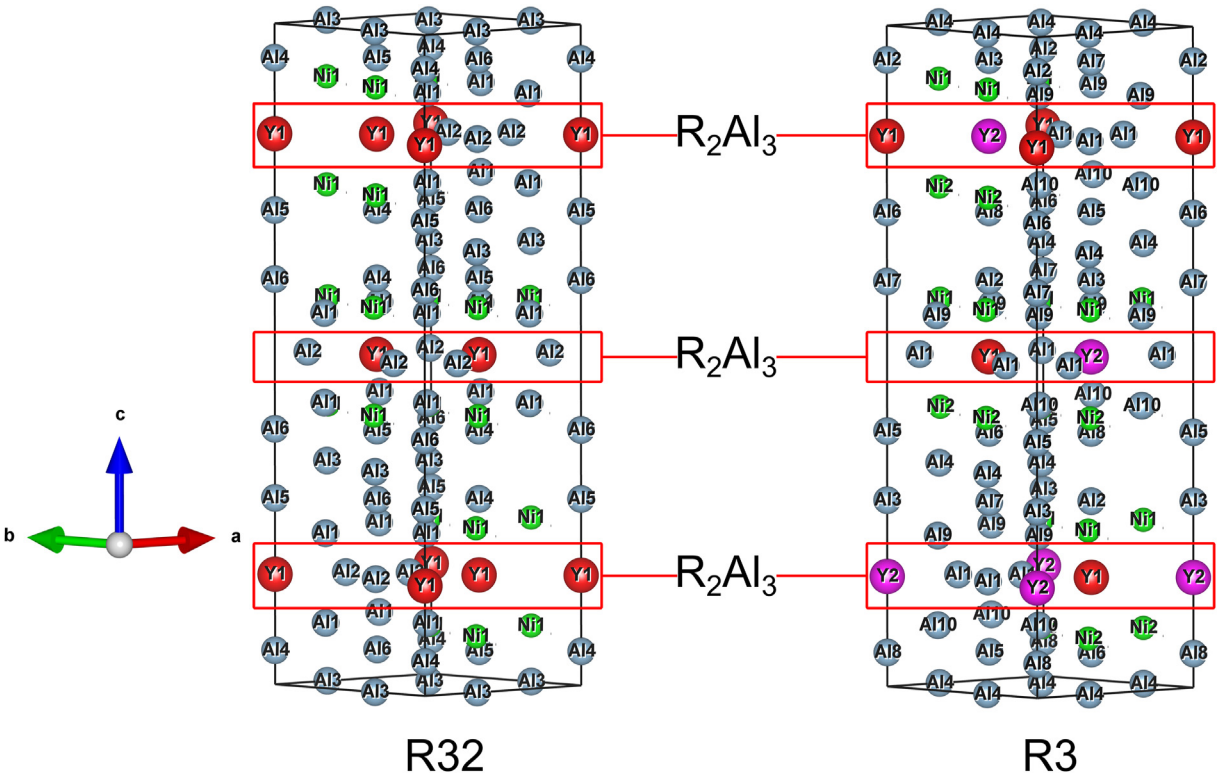

Fig.2. Projections of the unit cells of completely ordered models of the structure of YNi_3Al_9 compound in space groups *R32* and *R3*. The layers with composition R_2Al_3 highlighted.

3.2. *Physical properties and electronic structure calculations*

The title compound exhibits a metallic-like behavior with almost linear temperature dependence of electrical resistivity above 100 K (Fig. 3a). A residual resistivity ratio R(300 K)/R(1.8 K) ~ 18 is not large and might suggest possible scattering on imperfections within a unit cell.

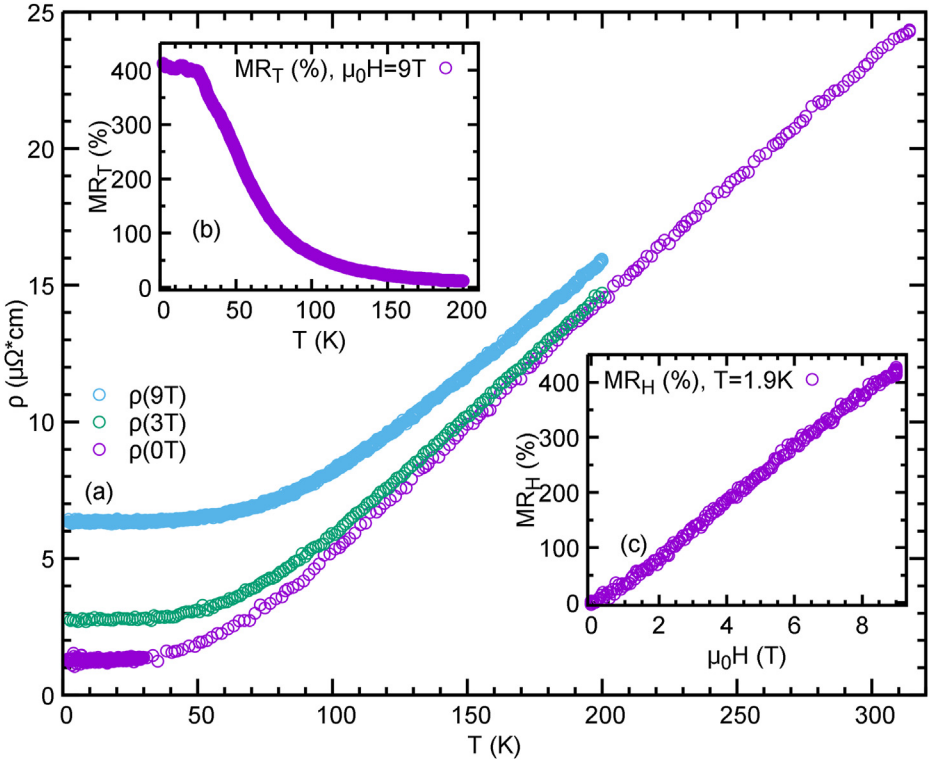

Fig.3. a) Temperature dependence of the electrical resistivity under various magnetic fields; b) temperature dependence of the magnetoresistance at 9T; c) field dependence of the magnetoresistance at T = 1.9 K.

Field and temperature dependent magnetoresistance were defined respectively:

$$MR_{H,1.9K} = \frac{(\rho_{H,1.9K} - \rho_{0,1.9K})}{\rho_{0,1.9K}} 100\% \quad (1)$$

$$MR_T = \frac{(\rho_{H,T} - \rho_{0,T})}{\rho_{0,T}} 100\% \quad (2)$$

where $\rho_{H,T}$ – electrical resistivity at given temperature at 9 T, $\rho_{0,T}$ – electrical resistivity at given temperature without magnetic field. These formulas were used in calculations of magnetoresistance.

YNi_3Al_9 reveals relatively high magnetoresistance (MR), as for the nonmagnetic intermetallics, its value reaches ~420% at 1.9 K under applied field of 9 T (Fig. 3 b). The MR(T) lowers slightly with temperature up to ~25K, then sharp decay is observed and at ~200K the magnetoresistance becomes negligible. The field dependent MR (measured at 1.9 K) is presented in Fig. 3 c. A linear increase of MR(H) with no traces of saturation or oscillations up to 9 T is observed.

Temperature dependence of the heat capacity C_p of YNi_3Al_9 between 2 K and 300 K is presented in Fig. 4 a. The heat capacity at high temperatures approaches Dulong-Petit limit, namely 3 nR = 324 J*mol^{-1}K^{-1}, where n = 13 – number of atoms per formula unit and R = 8.31 J*mol^{-1}K^{-1} – universal gas constant.

Temperature dependence of the heat capacity for low temperature range T = 1.8–8 K was approximated by the formula

$$C_p = \gamma T + \beta T^3 \quad (3)$$

where γ is Sommerfeld cefficient and β – phonon contribution to the heat capacity. The parameters γ and β were obtained from linear least squares fit of the latter formula (See Fig. 4 b). The Debye temperature of the YNi_3Al_9 compound was calculated on basis of the obtained value of β – phonon component of the heat capacity

$$\theta_D = \sqrt[3]{\frac{12\pi^4 nR}{5\beta}} \quad (4)$$

The solid black line represents a whole temperature fit to a combined model:

$$C_p = \gamma T + (1\text{-}k)C_{Einstein} + kC_{Debye} \quad (5)$$

Where γT is an electronic and $C_{Einstein}$ and C_{Debye} are phonon contributions to the specific heat given by:

$$C_{Einstein}(T) = 3nR\left(\frac{\theta_E}{T}\right)^2 \exp\left(\frac{\theta_E}{T}\right)\left[\exp\left(\frac{\theta_E}{T}\right) - 1\right]^{-2} \quad (6)$$

and

$$C_{Debye}(T) = 9nR\left(\frac{T}{\theta_D}\right)^3 \int_0^{\frac{\theta_D}{T}} \frac{x^4 \exp(x)}{[\exp(x) - 1]^2} dx \quad (7)$$

The characteristic temperatures obtained from the fit are $\theta_D = 480(6)$ K, $\theta_E = 198(8)$ K with the weight $k = 0.87(1)$. The Debye and Einstein parts are represented by a green and an orange line respectively in Fig. 4 a. The Debye temperature is relatively high and typical for the aluminides, as large concentration of light Al atoms causes high Debye temperature. The value of γ, estimated from the low temperature fit (discussed later) is more reliable, and hence in the fit procedure $\gamma = 5.9$ mJ mol^{-1} K^{-2} remained fixed.

Fig. 4 b shows the C_p/T vs. T^2 below 10 K. At sufficiently low temperatures C_p(T) can be described by $C_p(T) = \gamma T + \beta T^3$ and fitting our data (red solid line), we obtained $\gamma = 5.9$ mJ mol^{-1} K^{-2} and $\beta = 0.139(4)$ mJ/mol/K^4. Having β we can estimate the Debye temperature of YNi_3Al_9 using a relation

$$\theta_D = \sqrt[3]{\frac{12\pi^4 nR}{5\beta}} \quad (8)$$

The estimated $\theta_D = 566(5)$ K is higher than obtained from the whole temperature fit.

There is an another way to estimate Einstein temperature from the heat capacity measurement. Fig. 4 c shows temperature dependence of C_{phonon}/T^3, where C_{phonon} was obtained by subtraction γT from C_p. It can be shown that the maximum of $C_{Einstein}/T^3$ relation appears for $T_{max} = \theta_E/5$. Hence, $\theta_E = 5T_{max}$ and for YNi_3Al_9 $\theta_E = 205$ K in very good agreement with a value obtained for the whole temperature fit presented in Fig. 4 a.

An effort has been made to estimate electron-phonon coupling con-

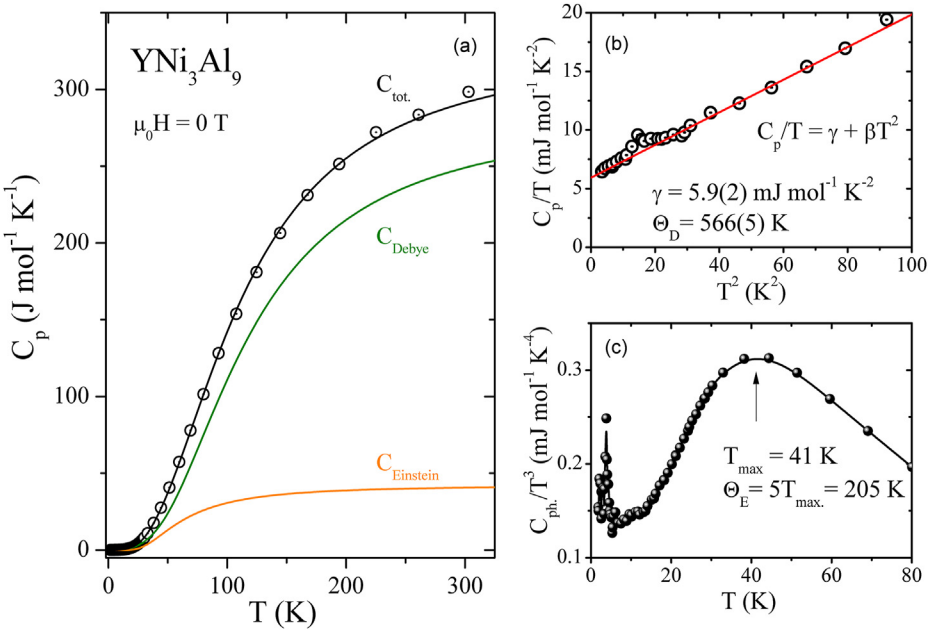

Fig.4. a) Temperature dependence of the heat capacity at zero magnetic field as well as Debye and Einstein contributions; b) low temperature fit C_p/T vs. T^2; c) phonon specific heat $C_{ph.}/T^3$ vs. temperature.

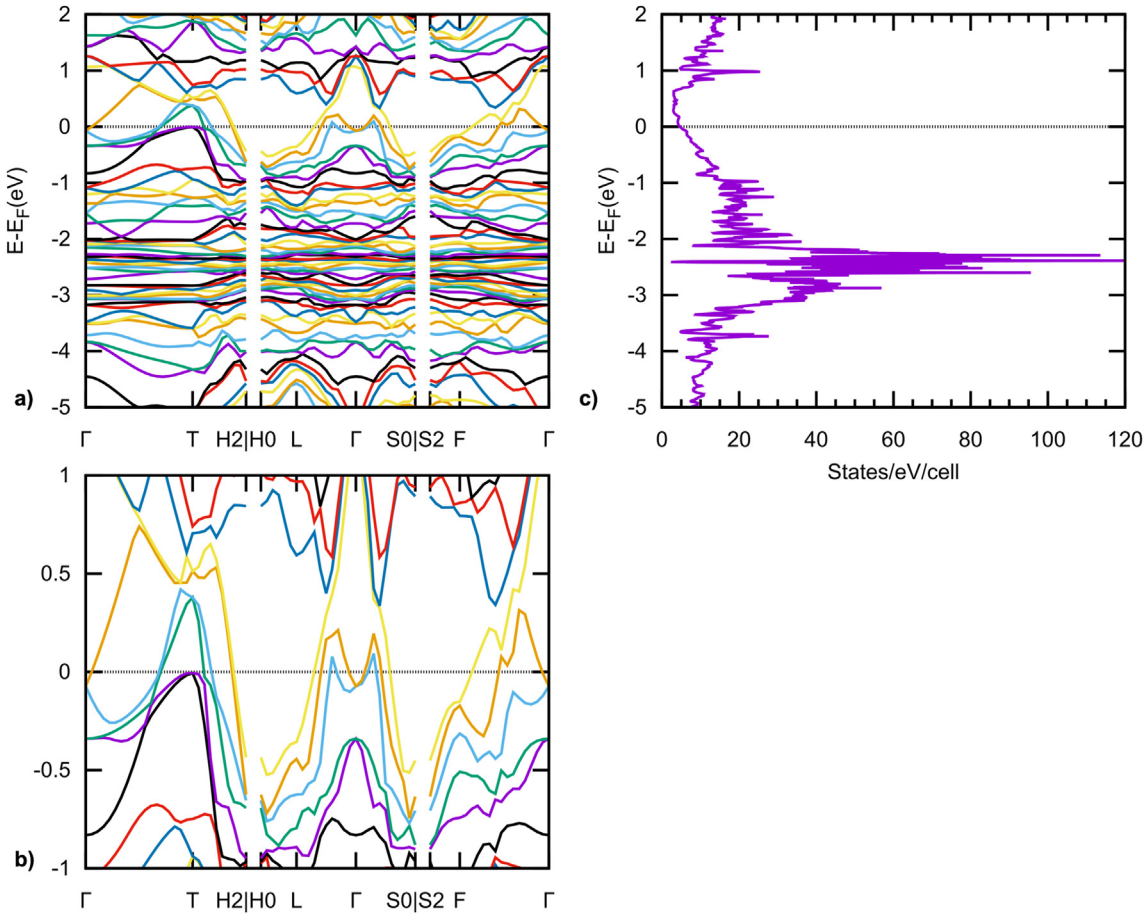

Fig.5. a) Band structure of the YNi_3Al_9 compound; b) finer details of the band structure; c) density of states of the YNi_3Al_9 compound.

stant and to estimate the possibility of superconductive transition in YNi_3Al_9. First of all "calculated" value of electron contribution into the heat capacity was obtained by McMillan formula

$$\gamma_{calc} = \frac{\pi^2}{3} k_B^2 * N(0) \tag{9}$$

where N(0) is number of the electrons on the Fermi level per 1 mol of the substance.

$$N(0) = \frac{DOS(E_F) * N_A}{Z} \tag{10}$$

where DOS(E_F) = 4.59 states/eV/cell – density of states at the Fermi level, N_A – Avogadro constant and $Z = 2$ – number of formula units per unit cell, used for calculations of DOS. After converting all of the units into SI, the following value of $\gamma_{calc} = 5.40$ mJ mol^{-1} K^{-2} was obtained. Subsequently, an estimate of electron-phonon coupling constant was calculated

$$\lambda = \gamma_{measured}/\gamma_{calc} - 1 = 0.092 \tag{11}$$

This value shows very weak electron-phonon coupling and is close to that of other aluminides. The obtained divisor under exponent

$$\lambda - \mu^*(1 + 0.62\lambda) = -0.0455 \tag{12}$$

in McMillan formula for critical temperature

$$T_C = \frac{\theta_D}{1.45} \exp\left[\frac{-1.04(1+\lambda)}{\lambda - \mu^*(1+0.62\lambda)}\right] \tag{13}$$

was negative, suggesting that the YNi_3Al_9 will not undergo superconducting transition.

The observed high values of magnetoresistance without any magnetic atoms stimulated interest to this phenomenon and therefore density of states and band structure calculations were carried out (See. Fig. 5). Band structure of the title compound revealed several important features, namely several very close bands, lying at the Fermi level near points Γ, F and Γ-T interval (See. Fig. 5 a, b). It is complex geometry of the Fermi surface that is likely responsible for the high magnetoresistance. The density of states plot shows metallic behavior of the title compound and the position of the Fermi level on the verge of a deep pseudogap substantiates possible charge transfer from yttrium to more electronegative nickel atoms, making the latter nonmagnetic. Similar partial charge transfer was predicted for other polar intermetallics, namely R-Zn-{Sn, Pb}, Li-Zn [33–39]. The DOS plots of the related Y–Ni–Al compounds, e.g. $Y_3Ni_5Al_{19}$ [40], have very similar shape with the exception of apparent pseudogap at the Fermi level.

4. Conclusions

Pure single crystals of the YNi_3Al_9 compound were grown by self-flux method from sample with initial composition Y:Ni:Al = 1:3:20 having excess of aluminum. These results indicate possible existence of region on phase diagram, where the title compound is in equilibrium with liquid. Single crystal X-ray diffraction data clearly show, that the structure of the studied sample is completely ordered and belongs to $ErNi_3Al_9$ type, space group *R32*, parameters of the unit cell $a = 7.2838(2)$ Å, $c = 27.4004(8)$ Å. Comparison of our results, obtained from flux-grown samples, was made with literature data for both flux-grown and arc melted samples. Clear

trend is visible towards formation of more ordered samples, while made by flux growth whereas formation of more disordered ones, while made by arc melting.

Electrical resistivity, magnetoresistance and heat capacity of the title compound were measured for the first time. It shows metallic-like behaviour and has very high values of magnetoresistance up to 420% at low temperatures. The observed very high magnetoresistance without presence of magnetic atoms can be explained by formation of Fermi surface pockets, which was substantiated by the results of band structure calculations.

The heat capacity approaches Dulong-Petit limit at high temperatures, while at the intermediate temperatures both dominating Debye and minor Einstein contributions to phonon heat capacity are observed. The calculated Debye temperature from low-temperature range θ_D = 566(5) K is significantly larger, than that from whole temperature range θ_D = 480(6) K and it is typical for aluminium-rich compounds. Corresponding Einstein temperature is θ_E = 198(8) K. The estimated value of electron-phonon coupling constant λ = 0.092 suggests very weak coupling.

CRediT authorship contribution statement

Igor Oshchapovsky: Conceptualization, Methodology, Validation, Formal analysis, Investigation, Data curation, Writing – original draft, Writing – review & editing, Visualization. **Ebube E. Oyeka:** Investigation, Resources, Data curation, Writing – review & editing, Visualization. **Thao T. Tran:** Validation, Formal analysis, Resources, Writing – review & editing. **Tomasz Klimczuk:** Conceptualization, Methodology, Validation, Formal analysis, Investigation, Resources, Data curation, Writing – review & editing, Visualization, Supervision. **Michał J. Winiarski:** Conceptualization, Methodology, Validation, Formal analysis, Investigation, Resources, Data curation, Writing – review & editing, Supervision.

Declaration of competing interest

The authors declare that they have no known competing financial interests or personal relationships that could have appeared to influence the work reported in this paper.

Data availability

Data will be made available on request.

Acknowledgments

This work was financed by the Gdansk University of Technology, Aurum Supporting International Research Team Building Project, no. 5/2020/IDUB/II.1.3, “Tuning the properties of quantum materials by the application of high pressure”, run within the frame of the Research University – Excellence Initiative. EEO and TTT thank the support from Clemson University, College of Science, Department of Chemistry.

Appendix A. Supplementary data

Supplementary data to this article can be found online at https://doi.org/10.1016/j.jssc.2023.123926.

References

[1] J.G. Kaufman, Introduction to Aluminum Alloys and Tempers, ASM International, 2000. ISBN 0-87170-689-X.
[2] F. Fiorillo, G. Bertotti, C. Appino, M. Pasquale, in: J.G. Webster (Ed.), Soft Magnetic Materials, Wiley Encyclopaedia of Electrical and Electronics Engineering, Wiley, 2016, https://doi.org/10.1002/047134608X.W4504.pub2.
[3] L. Boichyshyn, M. Kovbuz, O. Hertsyk, V. Nosenko, B. Kotur, Influence of structurization of amorphous metallic alloys $Al_{87}Y_{5-x}Gd_xNi_{8-y}$ (x = 0, 1, 5; y = 0, 4) on their mechanical properties, Phys. Solid State 55 (2013) 243–246, https://doi.org/10.1134/S1063783413020054.
[4] J.-M. Dubois, Properties- and applications of quasicrystals and complex metallic alloys, Chem. Soc. Rev. 41 (2012) 6760–6777, https://doi.org/10.1039/C2CS35110B.
[5] M.J. Kangas, D.C. Schmitt, A. Sakai, S. Nakatsuji, J.Y. Chan, Structure and physical properties of single crystal $PrCr_2Al_{20}$ and CeM_2Al_{20} (M=V, Cr): a comparison of compounds adopting the $CeCr_2Al_{20}$ structure type, J. Solid State Chem. 196 (2012) 274–281, https://doi.org/10.1016/j.jssc.2012.06.035.
[6] O. Moze, L.D. Tung, J.J.M. Franse, K.H.J. Buschow, Crystal structure and magnetic properties of CeV_2Al_{20} and $CeCr_2Al_{20}$, J. Alloys Compd. 268 (1998) 39–41, https://doi.org/10.1016/S0925-8388(97)00586-0.
[7] D. Puggioni, J.M. Rondinelli, Designing a robustly metallic noncenstrosymmetric ruthenate oxide with large thermopower anisotropy, Nat. Commun. 5 (2014) 3432, https://doi.org/10.1038/ncomms4432.
[8] P.W. Anderson, E.I. Blount, Symmetry considerations on martensitic transformations: "ferroelectric" metals? Phys. Rev. Lett. 14 (1965) 217–219, https://doi.org/10.1103/PhysRevLett.14.217.
[9] S. Bae, H. Kim, Y.S. Eo, S. Ran, I-lin Liu, W.T. Fuhrman, J. Paglione, N.P. Butch, S.M. Anlage, Anomalous normal fluid response in a chiral superconductor UTe_2, Nat. Commun. 12 (2021) 2644, https://doi.org/10.1038/s41467-021-22906-6.
[10] J. Prinz, O. Gröning, H. Brune, R. Widmer, Highly enantioselective adsorption of small prochiral molecules on a chiral intermetallic CompoundAngew, Chem., Int. Ed. Engl. 54 (13) (2015) 3902–3906, https://doi.org/10.1002/anie.201410107.
[11] R.E. Gladyshevskyy, K. Cenzual, H.D. Flack, E. Parthe, Structure of RNi_3Al_9 (R = Y, Gd, Dy, Er) with either ordered or partly disordered arrangement of Al-atom triangles and rare-earth-metal atoms, Acta Cryst B49 (1993) 468–474, https://doi.org/10.1107/S010876819201173X.
[12] O. Matselko, S. Pukas, Y. Lutsyshyn, R. Gladyshevskii, D. Kaczorowski, Ternary aluminides $R_{0.67}Ni_2Al_6$ (R=Sc, Y, Gd–Lu) with partly disordered structures, J. Solid State Chem. 198 (2013) 50–56, https://doi.org/10.1016/j.jssc.2012.09.031.
[13] T. Yamashita, R. Miyazaki, Y. Aoki, S. Ohara, Transport, thermal, and magnetic properties of $YbNi_3X_9$ (X=Al, Ga): a newly synthesized Yb-based Kondo lattice system, J. Phys. Soc. Jpn. 81 (2012), 034705, https://doi.org/10.1143/JPSJ.81.034705.
[14] S.G. de Mercena Propriedades estruturais e magneticas de compostos intermetalicos contendo terras raras, DISSERTACAO DE MESTRADO, UNIVERSIDADE FEDERAL DE SERGIPENUCLEO DE POS-GRADUACAO EM FISICA, Sao Cristovao-SE 2016, Brasil. https://ri.ufs.br/bitstream/riufs/5372/1/SAMUEL_GOMES_MERCENA.pdf.
[15] S.G. Mercena, J.G.S. Duque, L.S. Silva, R. Lora-Serrano, R.P. Amaral, J.M. Cadogan, D.J. Garcia, Doping the intermetallic compound ErNi3Al9 with Cu: a structural and magnetic characterization of a phase transition, J. Alloys Compd. 785 (2019) 105–109, https://doi.org/10.1016/J.JALLCOM.2018.12.342.
[16] P.H. Tobash, Yu Jiang, F. Ronning, C.H. Booth, J.D. Thompson, B.L. Scott, E.D. Bauer, Synthesis, structure and physical properties of $YbNi_3Al_{9.23}$, J. Phys. Condens. Matter 23 (8) (2011), 086002, https://doi.org/10.1088/0953-8984/23/8/086002.
[17] T. Mika, B. Kotur, Phase equlibria in the {Y, Gd}–Ni–Al ternary systems in the 65-100 at.% Al range at 773 K: a reinvestigation, Chem. Met. Alloys 3 (2010) 208–219, https://doi.org/10.30970/cma3.0171.
[18] R. Raggio, G. Borzone, R. Ferro, The Al-rich region in the Y-Ni-Al system: microstructures and phase equilibria, Intermetallics 5 (3) (2000) 247–257, https://doi.org/10.1016/S0966-9795(99)00100-4.
[19] J. Huang, B. Yang, H. Chen, H. Wang, Thermodynamic optimisation of the Ni-Al-Y ternary system, J. Phase Equilibria Diffus. 36 (4) (2015) 357–365, https://doi.org/10.1007/s11669-015-0390-6.
[20] Bruker AXS Inc, Madison, Wisconsin, USA, SAINT, 2014.
[21] Bruker AXS Inc, Madison, Wisconsin, USA, APEX2, SADABS, XPREP and SAINT-Plus, 2004.
[22] L. Palatinus, G. Chapuis, Superflip - a computer program for the solution of crystal structures by charge flipping in arbitrary dimensions, J. Appl. Cryst 40 (2007) 786–790, https://doi.org/10.1107/S0021889807029238.
[23] V. Petricek, M. Dusek, L. Palatinus, Crystallographic computing system JANA2006: general features, Z. Kristallogr. 229 (5) (2014) 345–352, https://doi.org/10.1515/zkri-2014-1737.
[24] P.J. Becker, P. Coppens, Extinction within the limit of validity of the Darwin transfer equations. I. General formalism for primary and secondary extinction and their applications to spherical crystals, Acta Cryst A30 (1974) 129–147, https://doi.org/10.1107/S0567739474000337.
[25] P.J. Becker, P. Coppens, Extinction within the limit of validity of the Darwin transfer equations. II. Refinement of extinction in spherical crystals of SrF_2 and LiF, Acta Cryst A30 (1974) 148–153, https://doi.org/10.1107/S0567739474000349.
[26] R. Sundararaman, K. Letchworth-Weaver, K.A. Schwarz, D. Gunceler, Y. Ozhabes, T.A. Arias, JDFTx: software for joint density-functional theory, SoftwareX 6 (2017) 278–284, https://doi.org/10.1016/j.softx.2017.10.006.
[27] K.F. Garrity, J.W. Bennett, K.M. Rabe, D. Vanderbilt, Pseudopotentials for high-throughput DFT calculations, Comput. Mater. Sci. 81 (2014) 446–452, https://doi.org/10.1016/j.commatsci.2013.08.053.
[28] J.P. Perdew, A. Zunger, Self-interaction correction to density-functional approximations for many-electron systems, Phys. Rev. B 23 (1981) 5048, https://doi.org/10.1103/PhysRevB.23.5048.
[29] G. Lehmann, M. Taut, On the numerical calculation of the density of states and related properties, Phys. Status Solidi 54 (1972) 469–477, https://doi.org/10.1002/pssb.2220540211.
[30] A.L. Spek, Single-crystal structure validation with the program PLATON, J. Appl. Cryst. 36 (2003) 7–11, https://doi.org/10.1107/S0021889802022112.

[31] V. Čavajda, P. Uhlík, A. Derkowski, M. Čaplovičová, J. Madejová, M. Mikula, T. Ifka, Influence of grinding and sonication on the crystal structure of talc, Clays Clay Miner 63 (2015) 311–327, https://doi.org/10.1346/CCMN.2015.0630405.
[32] F. Nakibuule, S.A. Nyanzi, I. Oshchapovsky, O.F. Wendt, E. Tebandeke, Synthesis of cyclic carbonates from epoxides and carbon dioxide catalyzed by talc and other phyllosilicates, BMC Chemistry 14 (2020) e61, https://doi.org/10.1186/s13065-020-00713-2.
[33] I. Oshchapovsky, V. Pavlyuk, G. Dmytriv, F. White, $LaZn_{12.37(1)}$, a zinc-deficient variant of the $NaZn_{13}$ structure type, Acta Crystallogr. E67 (2011), https://doi.org/10.1107/S1600536811028893 e i43.
[34] I. Oshchapovsky, O. Zelinska, B. Rozdzynska-Kielbik, V. Pavlyuk, Redetermination of $LaZn_5$ based on single crystal X-ray diffraction data, Acta Crystallogr. E68 (2012), https://doi.org/10.1107/S1600536811050987 e i1.
[35] A. Stetskiv, I. Tarasiuk, B. Rozdzynska-Kielbik, I. Oshchapovsky, V. Pavlyuk, Terbium (lithiumzinc) distannide, $TbLi_{1-x}Zn_xSn_2$ (x =0.2), Acta Crystallogr. E68 (2012), https://doi.org/10.1107/S1600536812002103 e i16.
[36] I. Oshchapovsky, V. Pavlyuk, G. Dmytriv, A. Griffin, Crystal structure of the $LaZn_4$ compound, Acta Crystallogr. C68 (2012), https://doi.org/10.1107/S0108270112020367 e i37-i40.
[37] I. Oshchapovsky, V. Pavlyuk, G. Dmytriv, B. Harbrecht, Pentalanthanum zinc diplumbide, $La_5Zn_{1-x}Pb_{2+x}$ (x≈0.6), Acta Crystallogr. E70 (2014), https://doi.org/10.1107/S1600536813033618 e i2-i3.
[38] I. Oshchapovsky, V. Pavlyuk, G. Dmytriv, Investigation of the compound $La_5Zn_{2-x}Pb_{1+x}$ (x=0.20-0.32), Z. Kristallogr. NCS. 233 (1) (2018) 83–84, https://doi.org/10.1515/ncrs-2017-0173.
[39] I. Oshchapovsky, S. Lidin, V. Pavlyuk, β-Li_2Zn_5 – a low symmetric polar intermetallic compound, Inorg. Chem. 58 (2019) 12590–12600, https://doi.org/10.1021/acs.inorgchem.9b01266.
[40] S. Dongwon, W.J. Golumbfskie, E.R. Ryba, L. Zikui, First-principles study of Al-Ni-Y ternary compounds for crystal structure validation, J. Alloys Compd. 462 (2008) 262–266, https://doi.org/10.1016/j.jallcom.2007.08.010.